

Modelling and prediction of the dynamic responses of large-scale brain networks during direct electrical stimulation

Presenter: Rongwei Liang (梁荣伟)

Date:6-26-2022

Yang Y, Qiao S, Sani O G, et al. Modelling and prediction of the dynamic responses of large-scale brain networks during direct electrical stimulation[J]. *Nature biomedical engineering*, 2021, 5(4): 324-345.



Outline

Prior work & Motivation

Methods and model evaluation

Results

Future directions



➤ Prior work about **direct electrical stimulation**

1. Observations modalities of direct electrical stimulation effect: local field potential (LFP), electrocorticogram (ECoG), functional magnetic resonance imaging (fMRI).

Basu, I. et al. Brain Stimul. 2019; Crowther, L. J. et al. Neurosci. Methods, 2019; Saenger, V. M. et al. Sci. Rep. 2017

2. Modelling the effect of stimulation from multiple brain regions activities (e.g. neuropsychiatric disorders)

Kirkby, L. A. et al. Cell, 2018

3. Computational modelling with biophysical insights (e.g. epilepsy modeling)

Sritharan, D. Neural Comput. 2014

➤ Motivation

1. Establishing the ability to predict how ongoing stimulation (input) drives the time evolution (that is, dynamics) of large-scale multiregional brain network activity (output) *remains elusive*.
2. **Precise neuromodulation in an individual** requires *the accurate modelling and prediction* of the effects of stimulation on the activity of their large-scale brain networks *is still unknown*.

Methods and modelling

➤ Modelling framework, neural recordings and stochastic stimulation input

multilevel noise (MN) [Yang, Y., J. Neural Eng. 2018](#)

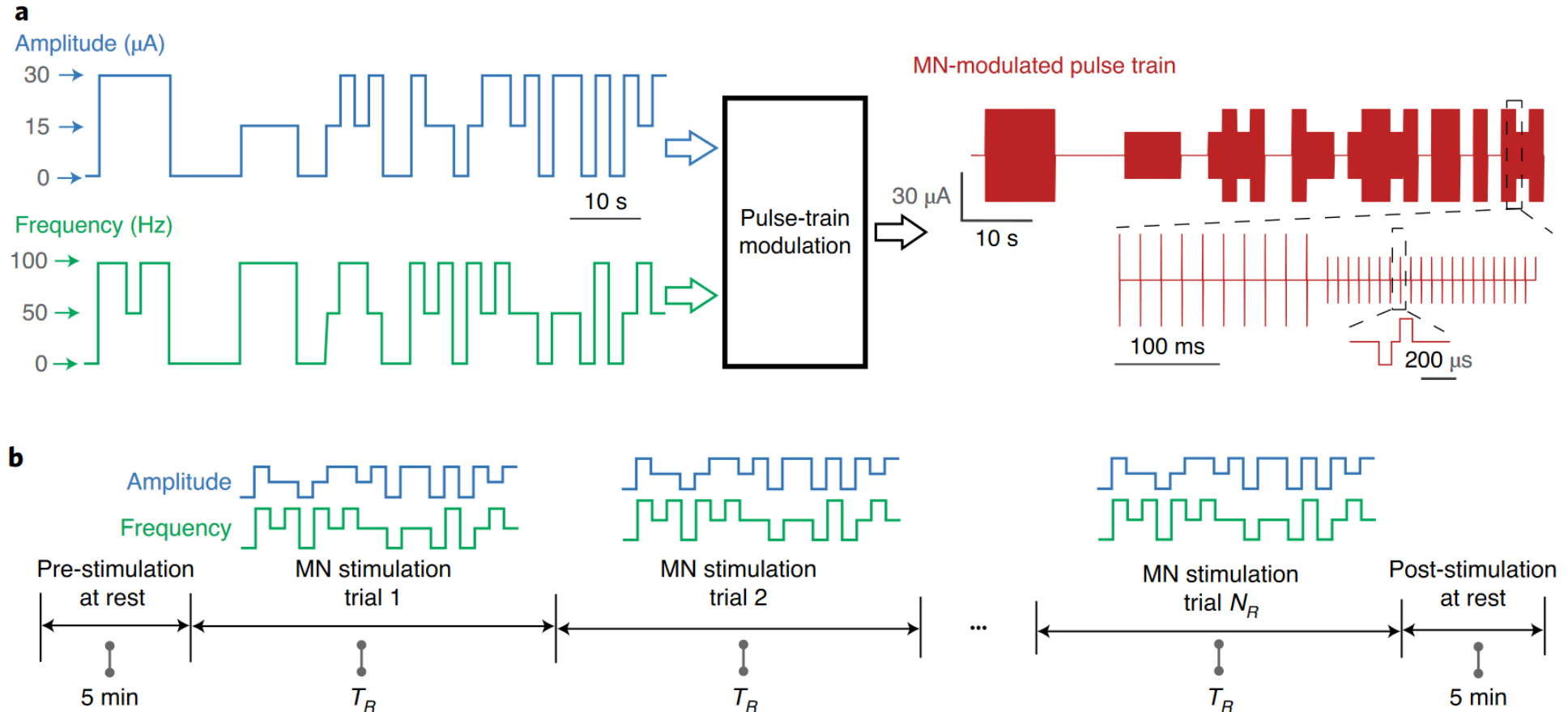


Fig. 1 | Input design, stimulation experiments and IO modelling framework.

Two male rhesus macaques (monkey A and M)

Methods and modelling

➤ Input-output (IO) modelling framework

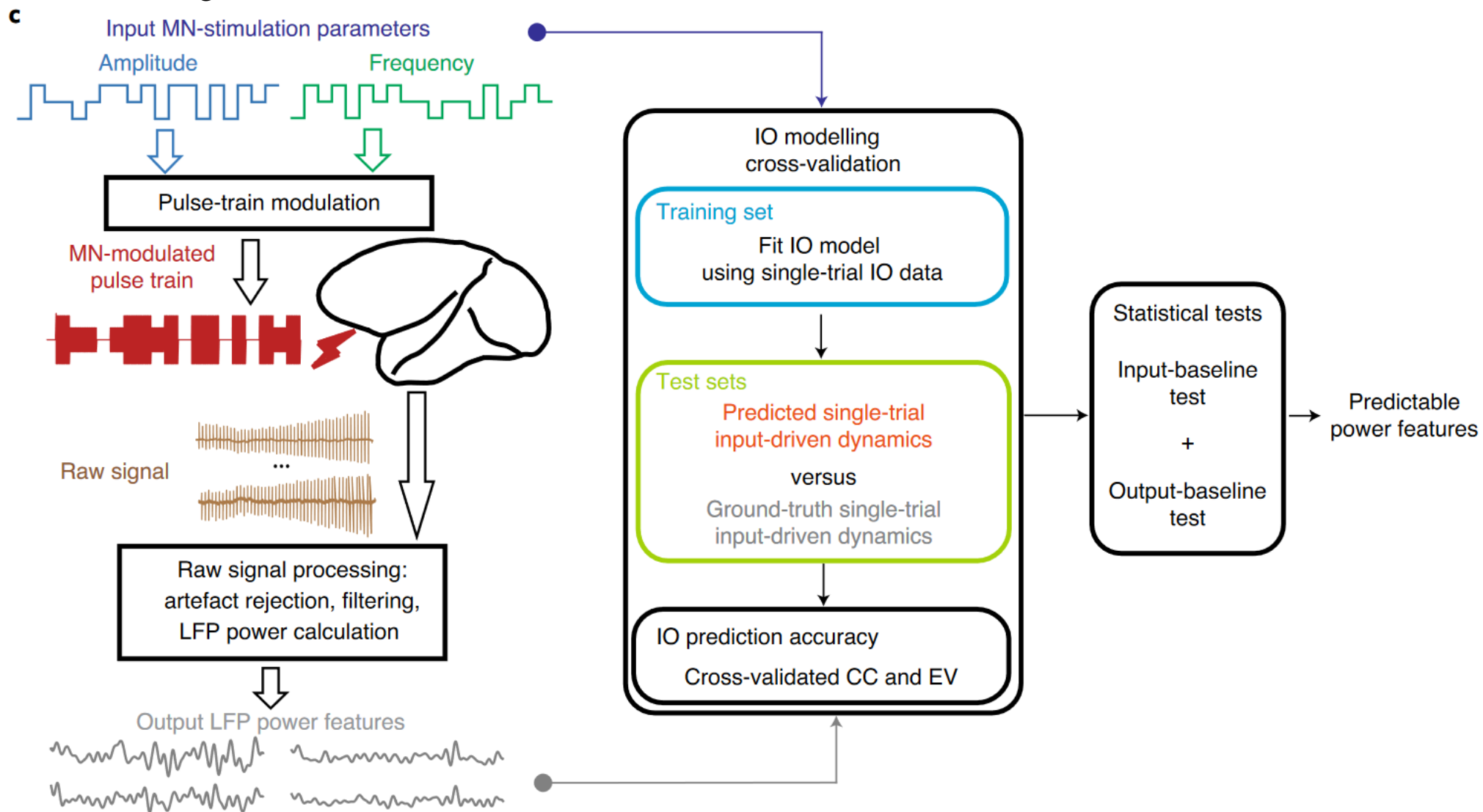


Fig. 1 | Input design, stimulation experiments and IO modelling framework.

Methods and modelling

➤ Dynamic input–output (IO) model structure

A dynamic multiple-input–multiple-output linear state-space mode(LSSM)

$$\begin{cases} \mathbf{x}_{k+1}^{(i)} = A^{(i)}\mathbf{x}_k^{(i)} + B^{(i)}\mathbf{u}_k + \mathbf{w}_k^{(i)} \\ \mathbf{y}_k^{(i)} = C^{(i)}\mathbf{x}_k^{(i)} + \mathbf{v}_k^{(i)} \end{cases}, \quad (1)$$

The i th LFP power features time series

A dynamic latent state

$\mathbf{u}_k = [u_k^{\text{amp}}, u_k^{\text{freq}}]'$ represent the stimulation amplitude and frequency, respectively

$\mathbf{w}_k^{(i)} \in \mathbb{R}^{N_x^{(i)} \times 1}$, $\mathbf{v}_k^{(i)} \in \mathbb{R}$ are zero-mean white Gaussian noise with covariance matrix $Q^{(i)} = \mathbb{E} \left[\begin{pmatrix} \mathbf{w}_k^{(i)} \\ \mathbf{v}_k^{(i)} \end{pmatrix} \begin{pmatrix} \mathbf{w}_k^{(i)'} & \mathbf{v}_k^{(i)'} \end{pmatrix} \right] \in \mathbb{R}^{(N_x^{(i)}+1) \times (N_x^{(i)}+1)}$.

$\theta^{(i)} = \{A^{(i)}, B^{(i)}, C^{(i)}, Q^{(i)}\}$

Methods and modelling

- Multi-trial experimental design to dissociate single-trial input-driven dynamics (Input-driven dynamics and intrinsic dynamics.)

The measured LFP power feature time series can be decomposed into two parts: $\mathbf{y}_k = \mathbf{y}_{k,I} + \mathbf{y}_{k,N}$

$$\textcircled{1} \text{ input-driven dynamics } \begin{cases} \mathbf{x}_{k+1,I} = A\mathbf{x}_{k,I} + B\mathbf{u}_k \\ \mathbf{y}_{k,I} = C\mathbf{x}_{k,I} \end{cases}, \quad (2)$$

$$\textcircled{2} \text{ intrinsic dynamics } \begin{cases} \mathbf{x}_{k+1,N} = A\mathbf{x}_{k,N} + \mathbf{w}_k \\ \mathbf{y}_{k,N} = C\mathbf{x}_{k,N} + \mathbf{v}_k \end{cases}, \quad (3)$$

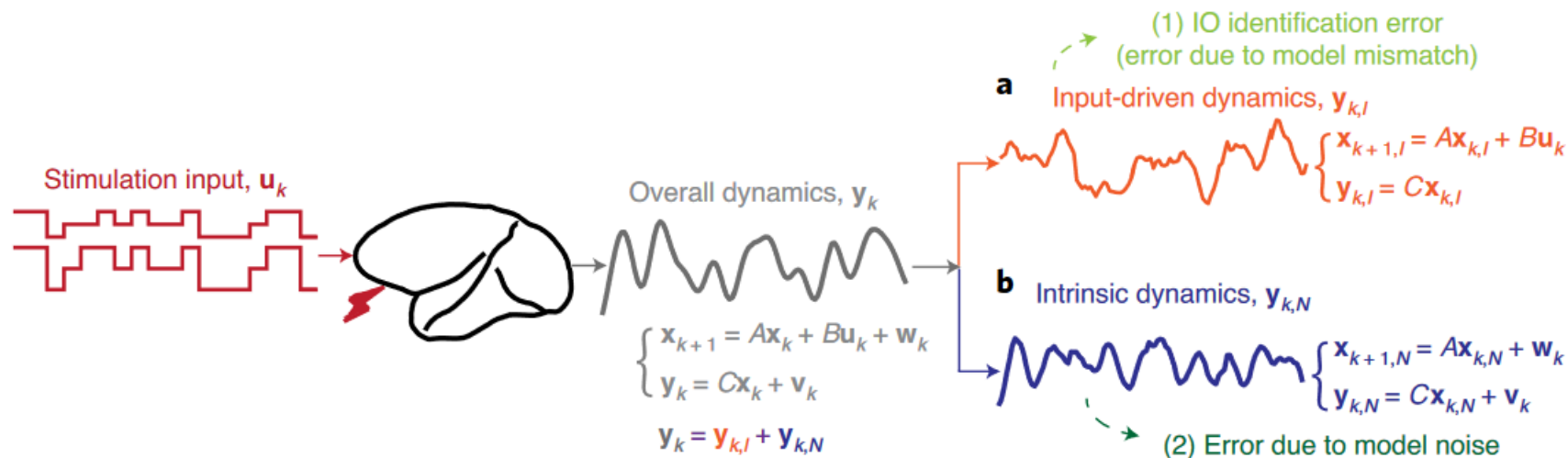


Fig. 7 | the overall brain network dynamics can be decomposed into input-driven dynamics and intrinsic dynamics to explain two possible sources for forward-prediction error. a,b,

➤ Model fitting in the training set

Used the prediction error method to fit the model parameters ($\theta = \{A, B, C, Q\}$)

$$J(\theta) = \sum_{h=1}^{N_R} \sum_{\{y_k, \mathbf{u}_k\} \in \mathcal{D}_h^{(\text{train})}} (\mathbf{y}_k - \hat{\mathbf{y}}_k(\theta))^2, \quad (11)$$

where $\hat{\mathbf{y}}_k(\theta)$ is the forward predictor in equation (6)

The fitted model parameters $\hat{\theta}$ via standard nonlinear optimization methods:

$$\hat{\theta} = \arg \min_{\theta} J(\theta), \quad (12)$$

the fitted model parameters



- Forward prediction to predict the single-trial input-driven dynamics in the test sets.

How well it can predict the input-driven dynamics in the test sets?

Forming a single-trial forward predictor based on equation (1)

$$\begin{cases} \mathbf{s}_{k+1} = A\mathbf{s}_k + B\mathbf{u}_k \\ \hat{\mathbf{y}}_k = C\mathbf{s}_k \end{cases}, \quad (4)$$

And the forward prediction of the latent state.

$$\mathbf{s}_k = B\mathbf{u}_{k-1} + AB\mathbf{u}_{k-2} + A^2B\mathbf{u}_{k-3} + \dots + A^{k-1}B\mathbf{u}_0 + A^k\mathbf{s}_0, \quad (5)$$

Where the past inputs $\{\mathbf{u}_0, \mathbf{u}_1, \mathbf{u}_2, \dots, \mathbf{u}_{k-1}\}$ and the initial state \mathbf{s}_0 and the forward prediction of LFP power feature $\hat{\mathbf{y}}_k$

$$\hat{\mathbf{y}}_k = CB\mathbf{u}_{k-1} + CAB\mathbf{u}_{k-2} + CA^2B\mathbf{u}_{k-3} + \dots + CA^{k-1}B\mathbf{u}_0 + CA^k\mathbf{s}_0. \quad (6)$$

➤ Model evaluation.

The linear correlation coefficient (CC) between the ground-truth single-trial input-driven dynamics and the predicted single-trial input-driven dynamics

$$\text{CC}^{\text{per fold}} = \frac{\text{Cov}\left(\{\hat{\mathbf{y}}_j\}, \{\bar{\mathbf{y}}_j\}\right)}{\sqrt{\text{Var}\left(\{\hat{\mathbf{y}}_j\}\right) \times \text{Var}\left(\{\bar{\mathbf{y}}_j\}\right)}}, \quad (7)$$

where $\text{Cov}(\cdot)$ and $\text{Var}(\cdot)$ represent the *empirical covariance* and *variance* of a time series, respectively.

The average CC over all 4 cross-validation folds:

$$\text{CC} = \frac{1}{4} \sum_{m=1}^4 \text{CC}^{(m)}, \quad (8)$$

A higher cross-validated CC represents better prediction and thus a higher IO prediction accuracy.

- To show the robustness of this paper's results

How much *variance* can be explained from the dynamic IO models.

$$\text{Explained variance} \longrightarrow \text{EV}^{\text{per fold}} = \left(1 - \frac{\frac{4}{L} \sum_{k=1}^{L/4} (\bar{y}_k - \hat{y}_k)^2}{\text{Var}(\bar{y}_k)} \right) \times 100\%, \quad (9)$$

The average EV over all four cross-validation folds for forward prediction

$$\text{EV} = \frac{1}{4} \sum_{m=1}^4 \text{EV}^{(m)}, \quad (10)$$

where $\text{EV}^{(m)}$ represents the EV in fold m as in equation (9).

Methods and modelling

- Evaluated the IO model in predicting the single-trial overall brain network dynamics.

One-step-ahead prediction of single-trial overall brain network dynamics during stimulation.

The optimal one-step-ahead prediction (minimize mean-squared error)

$$\begin{cases} \mathbf{z}_k = A\mathbf{z}_{k-1} + B\mathbf{u}_{k-1} + K(\mathbf{y}_{k-1} - C\mathbf{z}_{k-1}) \\ \tilde{\mathbf{y}}_k = C\mathbf{z}_k \end{cases}, \quad (13)$$

where \mathbf{z}_k is the one-step-ahead prediction of the latent state \mathbf{x}_k and K is the total Kalman gain

$$\begin{aligned} \tilde{\mathbf{y}}_k &= C\mathbf{B}\mathbf{u}_{k-1} + C(A - KC)\mathbf{B}\mathbf{u}_{k-2} + C(A - KC)^2\mathbf{B}\mathbf{u}_{k-3} \\ &+ \dots + C(A - KC)^{k-1}\mathbf{B}\mathbf{u}_0 + CK\mathbf{y}_{k-1} + C(A - KC)K\mathbf{y}_{k-2} \\ &+ C(A - KC)^2K\mathbf{y}_{k-3} + \dots + C(A - KC)^{k-1}K\mathbf{y}_0 \end{aligned} \quad (14)$$

Here the terms $C(A - KC)^{j-1}\mathbf{B}\mathbf{u}_{k-j}$ in the sum are evaluated from $j=1$ to k and similarly for terms associated with \mathbf{y}_{k-j} .

Results

➤ Prediction

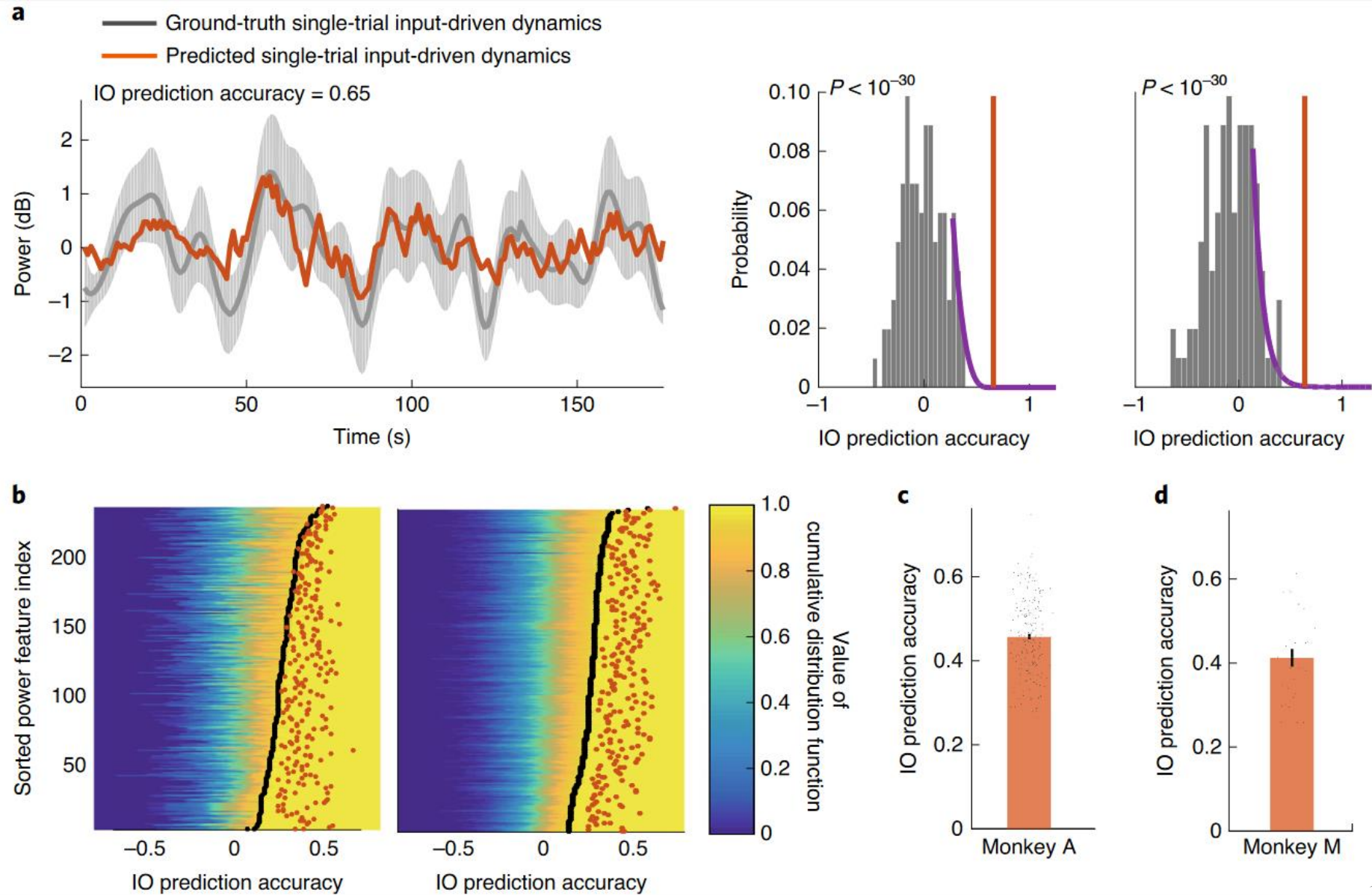


Fig. 2 | dynamic IO models accurately predict brain network dynamics in response to stimulation.

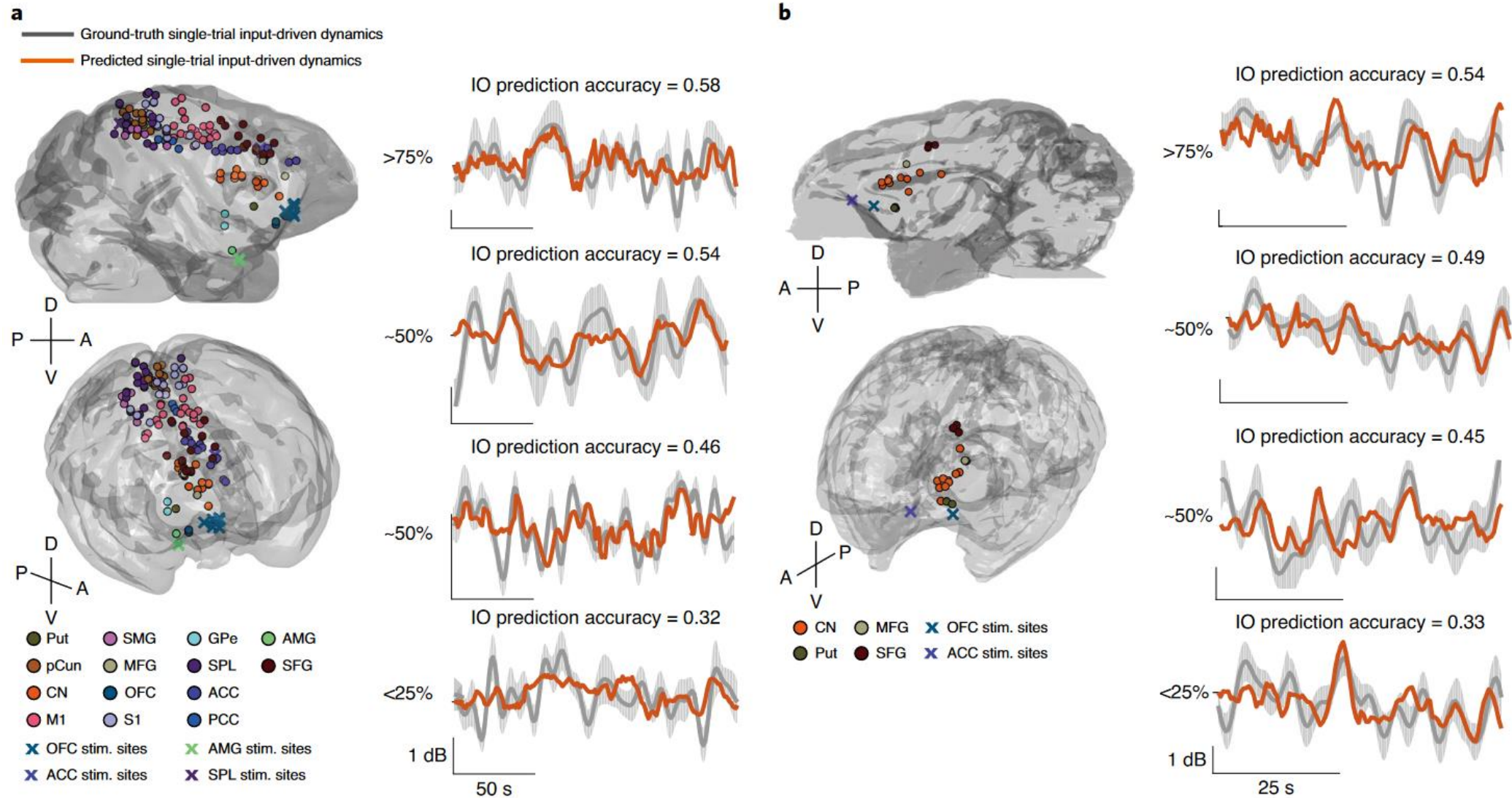


Fig. 3 | dynamic IO models predict the response to stimulation across multiple brain regions.

Results

➤ IO model for prediction

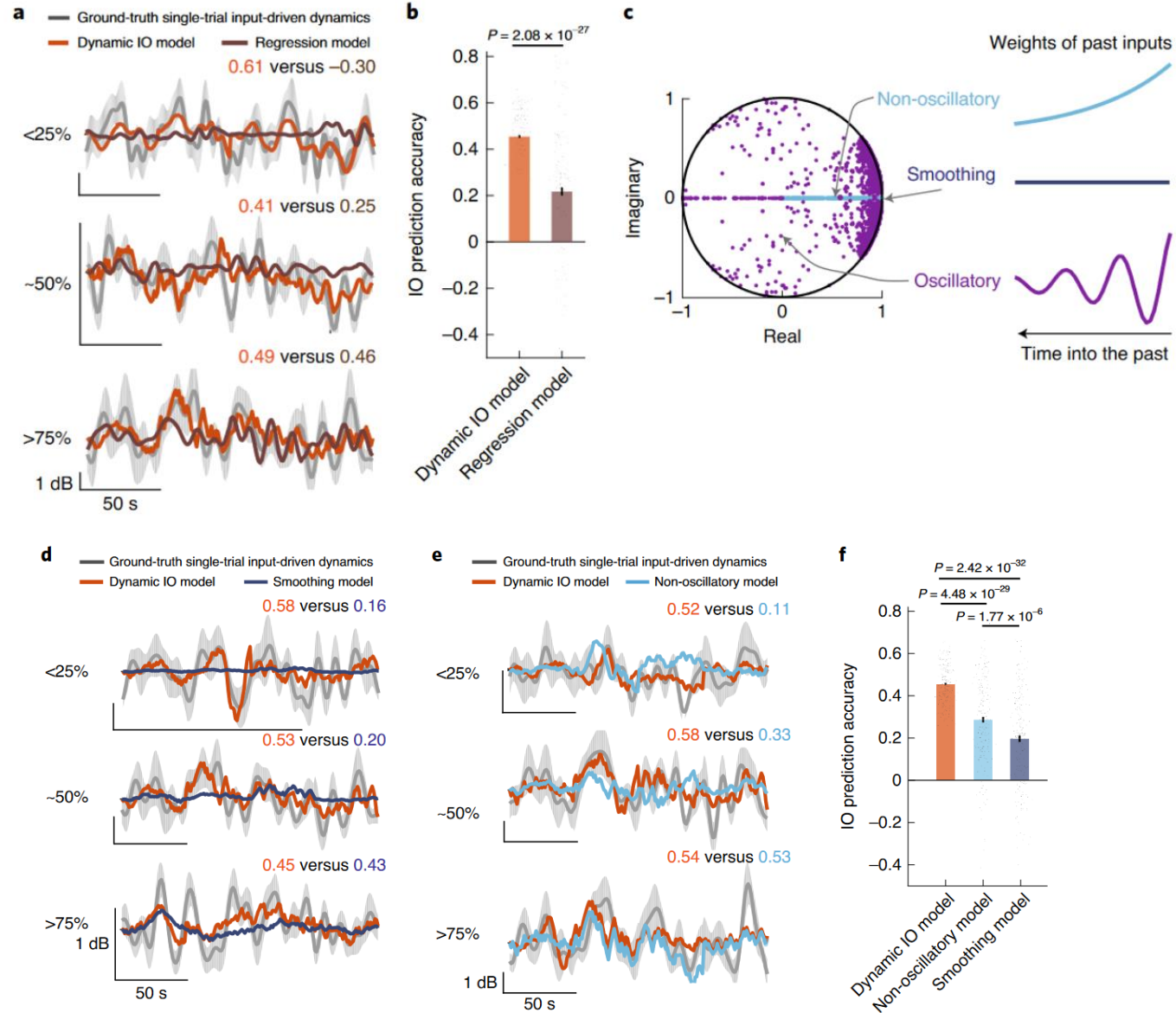


Fig. 4 | the dynamic structure of the IO model is essential for accurate prediction.

- Comparing to regression model, smoothing model, Non-oscillatory

Regression model, smoothing model and non-oscillatory model.

$$\mathbf{y}_k = \mathbf{B}\mathbf{u}_k + \mathbf{e}_k, \quad (15)$$

an overlapping window of $10T_s$ \Rightarrow $\mathbf{y}_k = \mathbf{B}\mathbf{u}_k$. (16)

a zero-mean Gaussian noise

The smoothing model is a special case of LSSM with **an identity state transition matrix**:

$$\begin{cases} \mathbf{x}_{k+1} = \mathbf{x}_k + \mathbf{B}\mathbf{u}_k + \mathbf{w}_k \\ \mathbf{y}_k = \mathbf{C}\mathbf{x}_k + \mathbf{v}_k \end{cases} \quad (17)$$

The non-oscillatory model is another special case of LSSM in which the state transition matrix \mathbf{A} in LSSM in equation (1) is constrained to have positive real eigenvalues

Methods and modelling

- Calculate at-rest functional controllability

$$\mathbf{z}_k = T\mathbf{z}_{k-1} + Dg_k, \quad (18)$$

where g_k is a nominal scalar variable representing the input strength and $\mathbf{z}_k = \begin{bmatrix} \mathbf{r}_k \\ \mathbf{p}_k \end{bmatrix}$

$D = [1, 1, 1, 1, 0, 0, \dots, 0]'$ is a nominal input matrix \rightarrow input g_k is delivered at the stimulation node.

Next, on the basis of equation (18), we calculated the infinite-horizon controllability Gramian W_c from T and D as the solution of the following discrete-time Lyapunov equation⁴⁶:

$$TW_cT' - W_c + DD' = 0. \quad (19)$$

$T \in \mathbb{R}^{(N_y+4) \times (N_y+4)}$ is **the state transition matrix** and is required to be **stable** (all eigenvalues within the unit disc)

➤ About at-rest functional controllability

Took the logarithm of the $(i + 4)$ th diagonal elements of W_c as the **functional controllability** from the stimulation node to the i th network node (note that the first 4 elements represent the stimulation node and *thus their controllability is not relevant to compute*):

$$O^{(i)} = \log(W_c(i + 4, i + 4)), i = 1, 2, \dots, N_y, \quad (20)$$

where $W_c(i, j)$ represents the i, j th element in the matrix W_c .

Methods and modelling

- Evaluate the relation of IO prediction accuracy and at-rest functional controllability.

① The relation of IO prediction accuracy and at-rest functional controllability

$$CC_{\text{region}}^{(j)} = a + bO_{\text{region}}^{(j)} \quad (21)$$

where the average at-rest functional controllability of the predictable power features within a brain region $O_{\text{region}}^{(j)}$ and $C_{\text{region}}^{(j)}$ is the corresponding average IO prediction accuracy, the corresponding average IO prediction accuracy as $CC_{\text{region}}^{(j)}$

② Whether an LFP power feature will have a predictable response or not?

$$\begin{cases} \mathcal{I}^{(i)} = 1, & \text{if } O^{(i)} > \sigma \\ \mathcal{I}^{(i)} = 0, & \text{if } O^{(i)} \leq \sigma \end{cases} \quad (22)$$

where $\mathcal{I}^{(i)} = 1$ represents a predictable i th LFP power feature and 0 otherwise.

③ If at-rest functional controllability can also predict the response strength of the network nodes?

the response strength

$$\mathcal{S} = \log \left(\frac{4}{L} \sum_{k=1}^{\frac{L}{4}} (\hat{y}_k)^2 \right), \quad (23)$$

where $\frac{L}{4}$ is the length of the test set.

Results

➤ At-rest functional controllability

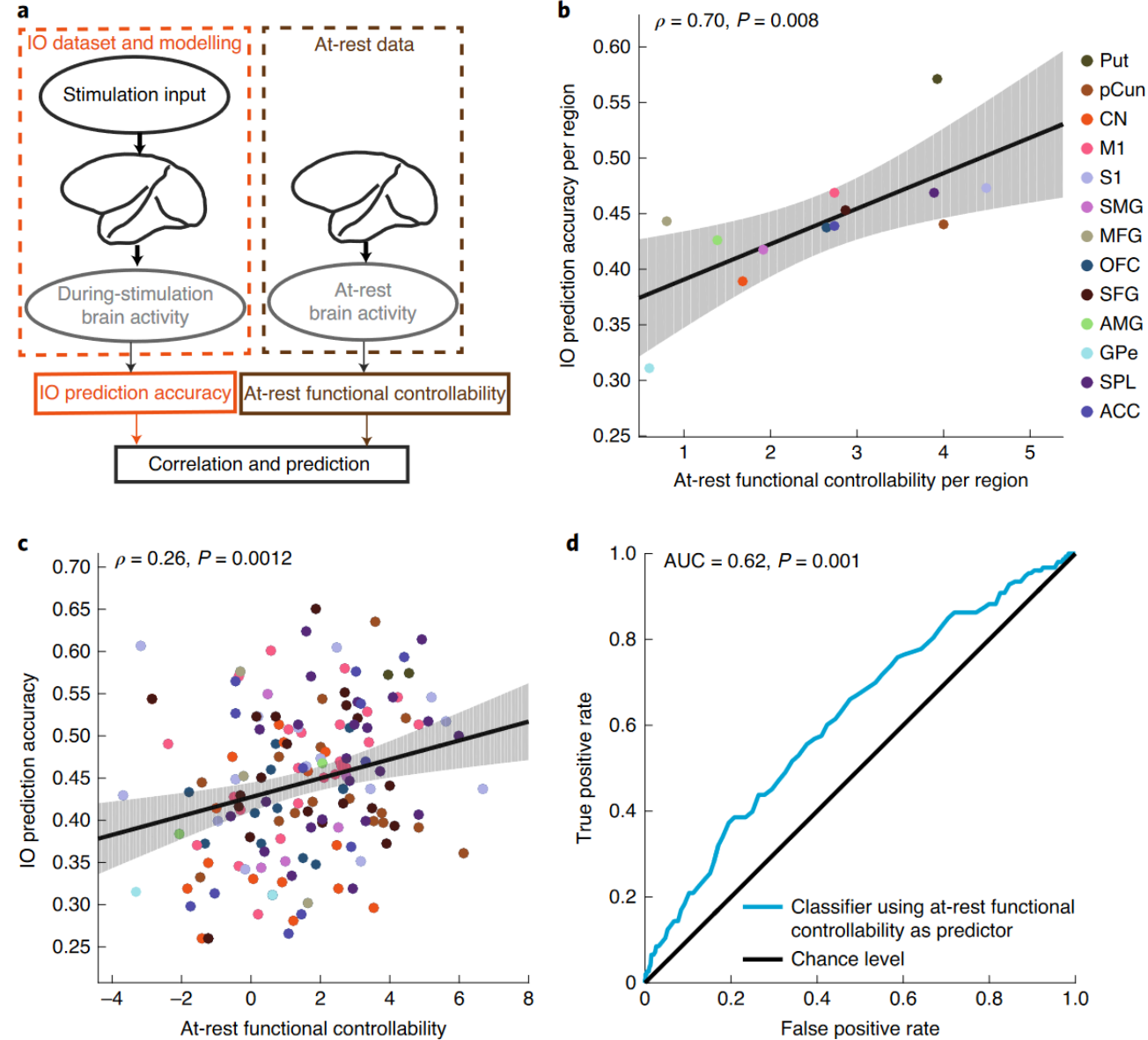


Fig. 5 | at-rest functional controllability explains the variability in the IO prediction accuracy at different network nodes.

- Compare to nonlinear IO model NLARX

NLARX model. The NLARX model structure¹¹⁸ models the output LFP power feature at each time k as

$$\mathbf{y}_k = \phi' \mathbf{R}_{N_a, N_b} + \sum_{m=1}^M \alpha_m \beta_m^{\frac{(N_a + N_b N_u)}{2}} \psi \left(\frac{\mathbf{R}_{N_a, N_b} - \boldsymbol{\gamma}_m}{\beta_m} \right), \quad (24)$$

$$\hat{\mathbf{y}}_k = \phi' \hat{\mathbf{R}}_{N_a, N_b} + \sum_{m=1}^M \alpha_m \beta_m^{\frac{(N_a + N_b N_u)}{2}} \psi \left(\frac{\hat{\mathbf{R}}_{N_a, N_b} - \boldsymbol{\gamma}_m}{\beta_m} \right), \quad (25)$$

$$\hat{\mathbf{R}}_{N_a, N_b} = \left[\hat{\mathbf{y}}_{k-1}, \hat{\mathbf{y}}_{k-2}, \dots, \hat{\mathbf{y}}_{k-N_a}, \mathbf{u}'_{k-1}, \mathbf{u}'_{k-2}, \dots, \mathbf{u}'_{k-N_b} \right]', \quad (26)$$

Results

➤ Nonlinear dynamic NLARX

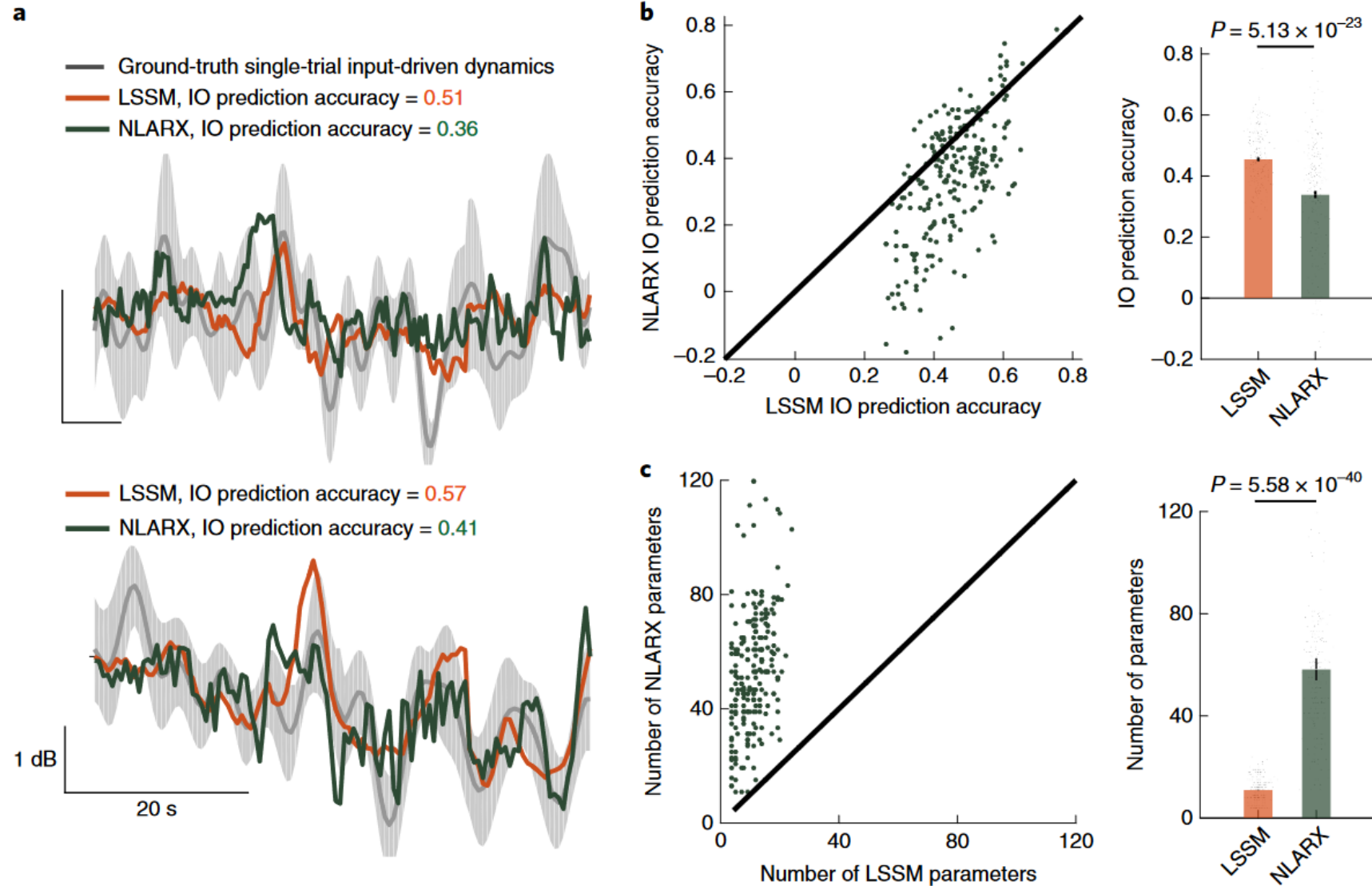


Fig. 6 | Nonlinear dynamic IO modelling does not outperform the linear dynamic IO models.

Results

➤ Visualisation of system response

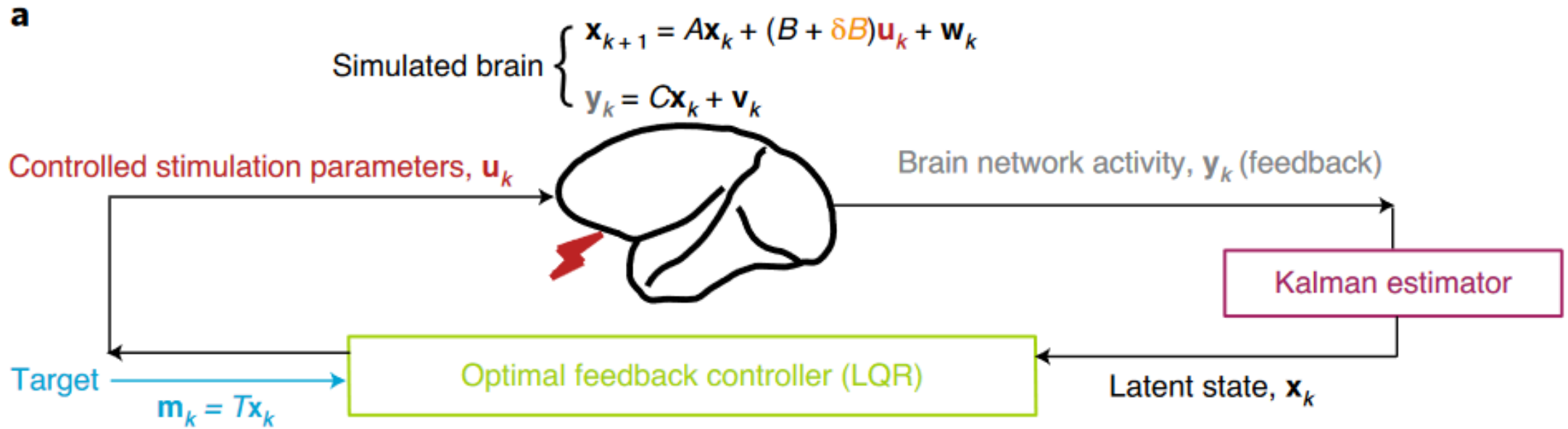


Fig. 8 | the fitted IO models enable closed-loop control of a simulated internal brain state.

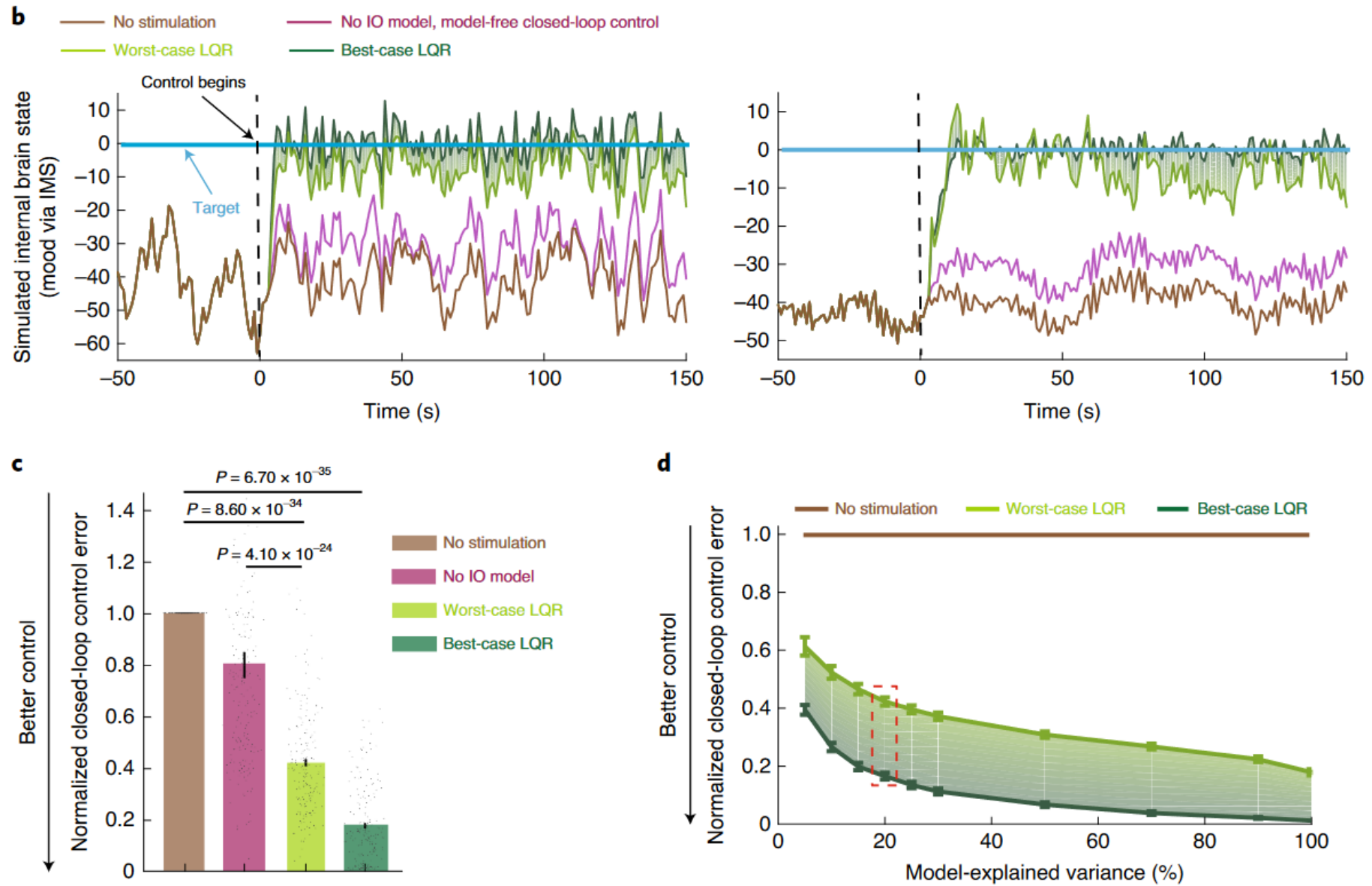


Fig. 8 | the fitted IO models enable closed-loop control of a simulated internal brain state.

Future directions.

1. General nonlinear IO modelling does not improve the linear dynamic IO model.
2. Future long-term chronic stimulation and recordings experiments can be used to further explore the nonlinearity in the IO response when more training data are available.



Your comment is highly appreciated!

Thank you for your attention

Further discussion



What is the application evaluation of clinical modulation with data-driven modeling and prediction of dynamical system?



In this study, the latent state in the proposed model does not have direct interpretation. How about the integration of prior knowledge in neuroscience for dynamical modeling?



How to figure out the high dimension and strong coupling properties in large-scale brain network?

Q&A